2ϕ is the phase of the backscattered signal relative to the reference signal at the detector.

To gain some insight as to the measurement error involved when the amplitude of the field is not constant over the dipole's excursions, let

$$f(t) \cong m_1 \cos(\omega_m t + \psi_1) - m_2 \cos(2\omega_m t + \psi_2). \quad (3)$$

The amplitude modulation indices at the fundamental and second harmonics of the dipole's frequency of vibration ω_m are $m_{1,2}$, respectively. $\psi_{1,2}$ are phase angles relative to the corresponding phase modulated terms. For simplicity, we further assume that the field's phase changes linearly with dipole displacement, so that

$$\phi(t) = 2\phi_m \cos(\omega_m t) \quad (4)$$

where ϕ_m ($= 2\pi d/\lambda$) is the maximum phase change. Retaining only the first three terms

$$\cos(2\phi + \phi(t)) = J_0(2\phi_m)\cos(2\phi) - 2J_1(2\phi_m)\sin(2\phi)\cos(\omega_m t) - 2J_2(2\phi_m)\cos(2\phi)\cos(2\omega_m t) \quad (5)$$

where J_n are Bessel functions of the first kind and order n. Inserting (3) and (5) into (2), the resulting filtered outputs of the narrowband amplifiers centered at ω_m and $2\omega_m$ are

$$V_1 = A_1 |F_x|^2 [(m_1/2)J_0(2\phi_m)\cos(2\phi)\cos(\omega_m t + \psi_1) - J_1(2\phi_m)\sin(2\phi)\cos(\omega_m t)] \quad (6)$$

and

$$V_2 = -A_2 |F_x|^2 \cos 2\phi [(m_2/2)J_0(2\phi_m)\cos(2\omega_m t + \psi_2) + J_2(2\phi_m)\cos(2\omega_m t)] \quad (7)$$

where the $A_{1,2}$ are constants which include the amplifier gains.

As shown in Fig. 1, V_1 is further processed by a limiter and a PSD. Ignoring the limiter for the moment, the dc output of the PSD is only that part of V_1 which is in phase with the audio frequency (AF) modulating signal $\cos \omega_m t$, or

$$\begin{aligned} V_1^{\text{PSD}} &= A_1' |F_x|^2 [(m_1/2)J_0(2\phi_m)\cos(2\phi)\cos(\psi_1) - J_1(2\phi_m)\sin(2\phi)] \\ &= A_1' |F_x|^2 \{[(m_1/2)J_0(2\phi_m)\cos\psi_1]^2 + J_1^2(2\phi_m)\} \\ &\quad \cdot \sin\left[2\phi - \tan^{-1}\left(\frac{m_1 J_0(2\phi_m)\cos\psi_1}{2J_1(2\phi_m)}\right)\right] \end{aligned} \quad (8)$$

where A_1' is a constant which includes the gain of the PSD. This signal is used to drive the servo which seeks a zero crossing of (8) by changing the phase, ϕ. This occurs at

$$2\phi_0 = \tan^{-1}\left(\frac{m_1 J_0(2\phi_m)\cos\psi_1}{2J_1(2\phi_m)}\right). \quad (9)$$

The zero crossings and subsequent phase error are not affected by the limiter which simply prevents the PSD from being overdriven.

If the amplitude modulation is very small, or if $2\phi_m \simeq 2.4$ so that $J_0 \cong 0$, these zero crossings are shifted only slightly from $\pm n\pi$ where the crossings would have been if there were no amplitude modulation. Furthermore, if $2\phi_m \cong 2.4$ the amplitude error in V_2 given by (7) is also minimized, but this condition may be difficult to maintain if the phase variation is nonlinear.

If amplitude modulation is not considered, the dipole's excursion would normally be adjusted so that $J_2(2\phi_m)$ is maximum ($2\phi_m = 3.1$). Then $J_0(3.1) = -0.292$, $J_1(3.1) = 0.3$, and taking $\psi_1 = 0$ in (9), the phase error is $2\phi_0 = -8.3°$ if $m_1 = 0.3$. Also, note that the peak-to-peak phase change is almost π. Further, such a large dipole excursion can lead to significant second harmonic amplitude modulation, i.e., m_2. In turn, this leads to an amplitude measurement error using V_2.

These amplitude and phase errors can also be reduced by interchanging the roles of V_1 and V_2, at least in cases where the phase changes linearly. To show this, V_2 is coherently compared with $\cos(2\omega_m t)$ by a PSD detector. Some PSD's (e.g., a lock-in amplifier) are capable of doing this by using the fundamental $\cos \omega_m t$ reference signal. Then the dc output of this PSD is

$$V_2^{\text{PSD}} = A_2' |F_x|^2 \cos(2\phi)[(m_2/2)J_0(2\phi_m)\cos\psi_2 + J_2(2\phi_m)]. \quad (10)$$

When this signal is fed to the servo, the system will stabilize so that $\cos 2\phi_0 = 0$, or $2\phi_0 = \pm(2n+1)\pi/2$ regardless of the amplitude modulation. The servo position is therefore a direct indicator of the correct phase.

The relative field amplitude is indicated by V_1. For $\cos 2\phi_0 = 0$, (6) becomes

$$V_1 = -A_1 |F_x|^2 J_1(2\phi_m)\cos\omega_m t$$

which is also independent of the incidental amplitude modulation.

An additional benefit of using V_1 to measure amplitude and V_2 to control the phase via the servo is that the phase modulation index $2\phi_m$ can be somewhat less than when their roles are reversed. For example, $J_1(2\phi_m)$ is maximum for $2\phi_m = 1.84$ which is significantly less than the value of 3.1 which is required to make $J_2(2\phi_m)$ maximum.

REFERENCES

[1] N. A. Mathews and H. Stachera, "A vibrating-dipole technique for measuring millimeter-wave fields in free space," *IEEE Trans. Microwave Theory Tech.*, vol. MTT-22, pp. 103–110, Feb. 1974.

[2] ——, "An automatic system for simultaneous measurement of amplitude and phase of millimeter-wave fields," *IEEE Trans. Microwave Theory Tech.* (Short Papers), vol. MTT-22, pp. 140–142, Feb. 1974.

[3] J. H. Richmond, "Measurement of time-quadrature components of microwave signals," *IRE Trans. Microwave Theory Tech.*, vol. MTT-3, pp. 13–15, Apr. 1955.

[4] ——, "A modulated scattering technique for measurement of field distributions," *IRE Trans. Microwave Theory Tech.*, vol. MTT-3, pp. 13–15, July 1955.

[5] J. D. Dyson, "The measurement of phase at UHF and microwave frequencies," *IEEE Trans. Microwave Theory Tech.*, vol. MTT-14, pp. 410–423, Sept. 1966.

[6] R. J. King, "Real-time measurement of microwave parameters and EM fields," *IEEE Trans. Instrum. Meas.*, vol. IM-21, pp. 2–11, Feb. 1972.

[7] D. L. Jaggard and R. J. King, "Sensitivity and dynamic range considerations for homodyne detection systems," *IEEE Trans. Instrum. Meas.*, vol. IM-22, pp. 331–338, Dec. 1973.

[8] F. Reggia and E. G. Spencer, "A new technique in ferrite phase shifting for beam scanning of microwave antennas," *Proc. IRE*, vol. 45, pp. 1510–1517, Nov. 1957.

[9] I. Barbash and J. J. Maune, "A waveguide latching ferrite phase shifter," in *Proc. IEEE G-MTT Int. Microwave Symp.* (Detroit, MI, May 1968).

Time-Domain Measurement of Loss and Dispersion

D. A. LUCE, H. M. CRONSON, SENIOR MEMBER, IEEE, AND P. G. MITCHELL, MEMBER, IEEE

***Abstract*—Time-domain metrology (TDM) techniques are applied to determine loss and dispersion in microstrip and coaxial cable for possible future use in interconnections in the frequency range of 0.4–10 GHz. After a brief presentation of the method, results are given for microstrip, RG/U 58, and RG/U 188A coaxial cable. Good agreement is obtained between measured, computed, and published values. Major advantages of the technique are that unwanted multiple reflections can be excluded from the measurement time window, and errors from interface discontinuities can be evaluated and removed from the final result.**

Manuscript received October 14, 1974; revised June 2, 1975.

D. A. Luce was with the Sperry Research Center, Sudbury, MA 01776. He is now with Moog Music, Inc., Williamsville, NY 14221.

H. M. Cronson and P. G. Mitchell are with the Sperry Research Center, Sudbury, MA 01776.

I. INTRODUCTION

Recently we have become interested in finding quick and accurate procedures to assess the microwave properties of interconnection cables. In this short paper we report on the very useful method of employing time-domain techniques to obtain frequency-domain characteristics. Time-domain reflectometry has been in wide use for over a decade for locating discontinuities in transmission lines [1]. Although this short paper is primarily concerned with determining loss and dispersion in microstrip and coaxial cables between 0.4 and 10 GHz, it should be noted that time-domain metrology (TDM) has found wide application in materials and microwave component measurements [2], [3]. The calculation of frequency-domain data from transient responses comes directly from the identity between a device's transfer function and the Fourier transform of its impulse response. In essence, TDM characterizes a component by its transient response to a subnanosecond baseband pulse. The waveforms are acquired by a sampling oscilloscope with a computer-controlled closed-loop scan. The sampled time-domain points are then translated into the frequency domain via the fast-Fourier-transform method, and relevant scattering parameters are computed. A major advantage of TDM in transmission line testing is that unwanted responses can be excluded from the measurement time window.

II. EXPERIMENTAL PROCEDURE

The method can best be understood with reference to Fig. 1 which illustrates the experimental configuration and observed waveforms for microstrip testing. The pulse generator produces a 6-V smoothed impulse with about a 70-ps half-width using an avalanche transistor and step-recovery diodes [4]. A portion of this pulse is also introduced as a reference signal in channel B of the sampling head to reduce the long-term drift and jitter of the oscilloscope waveforms [2]. The air delay lines are used to keep unwanted reflections from the two 2.5-ns-wide measurement time windows, T_1 and T_2. In the experimental procedure, three initialization and two test waveforms are acquired. The initialization signals are an incident waveform and two background scans. The test waveforms are the reflections from the input connector of the line under test and the reflection from the shorted end of the line. For accurate measurements the small residual background level due to ripples in the wake of the reference pulse and minor reflections between the generator and sampling head are removed from the principal scans. Errors due to imperfect connectors are also removed from the raw data using the input connector reflection. In Fig. 1 a short circuit is first connected at the end of the second air line, and the waveform $v_1(t)$ in time window T_1 is scanned and digitized. Next, the short is removed and replaced by a 50-Ω termination. The background waveforms $v_{1b}(t)$ and $v_{2b}(t)$ in T_1 and T_2, respectively, are then acquired for later subtraction from the main signals. Lastly, the microstrip under test is attached to the line while the reflection from the coaxial-to-microstrip adapter $v_{1a}(t)$ is scanned in time window T_1, and the return from the short in the board $v_{2r}(t)$ is acquired in T_2. Additional boards may also be tested without repeating the three initialization measurements.

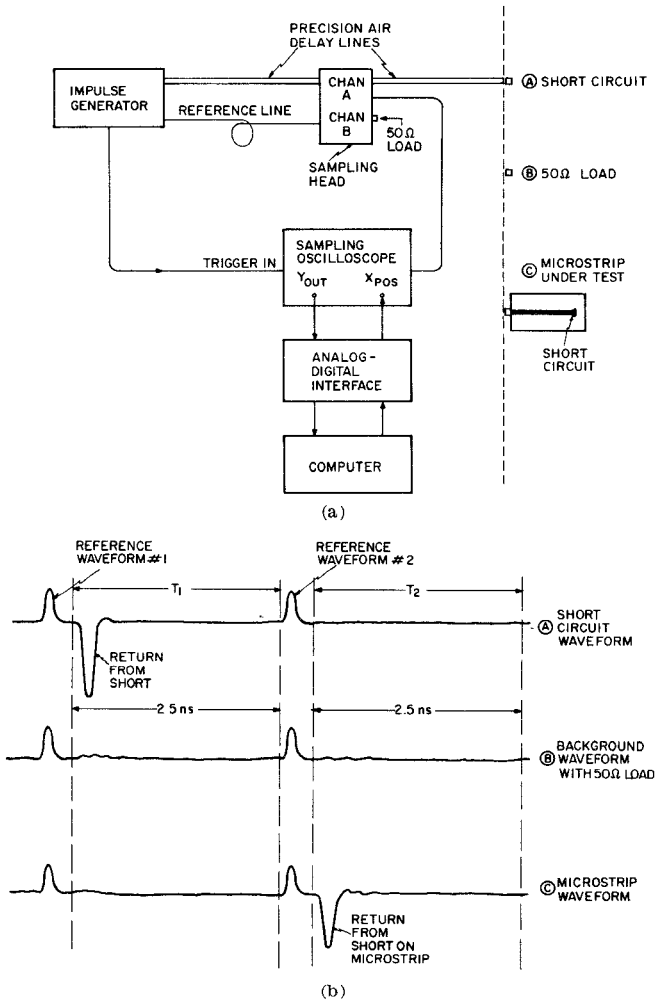

Fig. 1. Measurement configuration and relevant waveforms. (a) Experimental configuration. (b) Sampling oscilloscope waveforms in the channel A and channel B mode.

These acquired waveforms can be related to the microstrip properties with reference to the bounce diagram in Fig. 2. In the figure it is assumed that the impedance of the microstrip is close to 50 Ω and the connector contributes a shunt reactive discontinuity with a complex reflection coefficient of $\rho(\omega)$, where ω is the radian frequency. Using $T(\omega)$ as the one-way-propagation complex loss coefficient, the signal emerging after reflection from the short on the circuit board is seen to be $-T^2(1+\rho)^2$. The reflection coefficient $\rho(\omega)$ is related to the acquired waveforms by

$$\rho(\omega) = \frac{V_\rho(\omega)}{V_i(\omega)}$$

where the reflected signal is given by the identity

$$V_\rho(\omega) \equiv F\{v_{1a}(t) - v_{1b}(t)\}$$

and $F\{\ \}$ defines the discrete Fourier transform of the sampled time function within the curly brackets. Similarly, the incident signal in the frequency domain is defined by

$$V_i(\omega) \equiv F\{-v_1(t) - v_{1b}(t)\}.$$

The signal which twice traverses the board under test is given by the

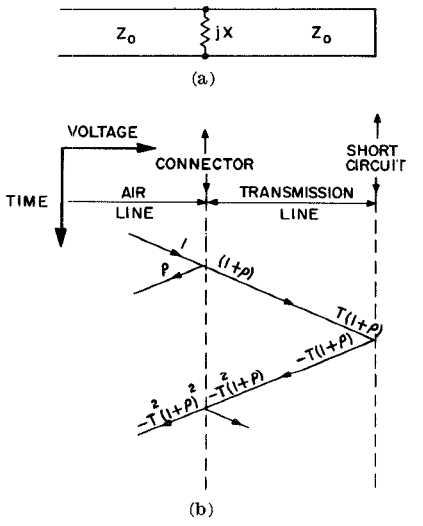

Fig. 2. Circuit representation and reflections of test lines. (a) Transmission lines. (b) Bounce diagram.

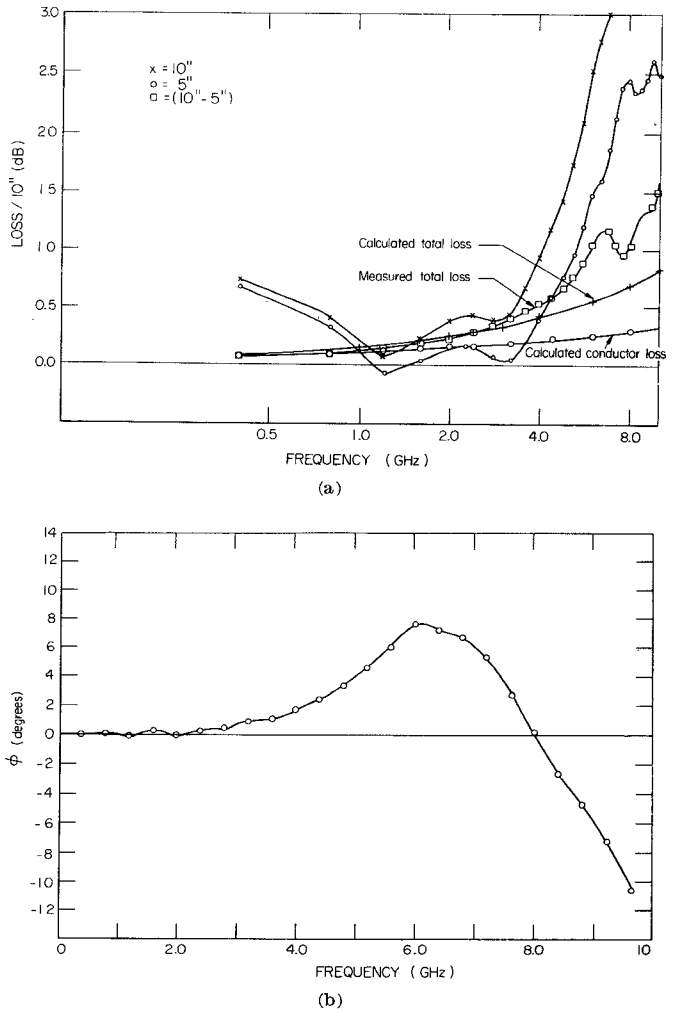

Fig. 3. Attenuation and normalized phase shift versus frequency for PTFE microstrip. (a) Measured and calculated attenuation for 5-in and 10-in microstrip and their difference. (b) Normalized phase shift.

equation

$$-T^2(1+\rho)^2 = \frac{V_T(\omega)}{V_i(\omega)}$$

where

$$V_T(\omega) \equiv F\{v_{2r}(t) - v_{2b}(t)\}.$$

Therefore, the transmission loss can be expressed as

$$T^2 = -\frac{V_T}{V_i} \times \frac{1}{(1+V_\rho/V_i)^2}.$$

In practice, after the five waveforms are digitized and the background subtractions made, fast Fourier transforms are performed and the necessary divisions are computed. The output is printed out on a teletype showing loss in dB and relative phase angle in degrees as a function of frequency. In an alternative testing procedure, two identical boards of different length may be measured without accounting for connector mismatch. Since the reflection term is common to both measurements, it will cancel out in the final results.

III. RESULTS

To illustrate typical data obtainable with these methods, results are given below for a polytetrafluorethylene (PTFE) microstrip, RG/U 58, and RG/U 188 coaxial cable.

A. PTFE Microstrip

The loss and dispersion characteristics of PTFE microstrip were measured by noting the difference in attenuation and phase shift between a 10-in and a 5-in length of 50-Ω microstrip on the same piece of circuit board with identical Omnispectra miniature (OSM) interconnections to the measurement system. The 10-in board was connected and a measurement of the pulse after traversing 20 in of board length (down and back) was obtained. This measurement was then repeated with the line shorted at the 5-in mark.

Fig. 3(a) shows the attenuation results for the 10-in board, the 5-in board, and the difference between the two. It should be noted that while the absolute values for the 5- and 10-in boards were erratic, the difference curve is monotonic to about 6 GHz. In this differential measurement, corrections for losses at the system–board interface are not required. The erratic behavior, especially the rapidly increasing losses at the high-frequency end of the curves for the individual lines, is due primarily to losses/reflections at the system–circuit-board interface.

Fig. 3(a) also shows the calculated conductor loss and the dielectric loss using equations given in Pucel *et al.* [5], based on the loss tangent value of 0.0018 specified by the manufacturer of this board. The calculated and observed values are within experimental error up to 3 GHz. As expected, the loss up to 1.0 GHz is primarily conductor loss.

Fig. 3(b) is a normalized (delay removed) plot of phase shift versus frequency of the PTFE microstrip. These phase shifts can be converted to propagation velocities using the equation

$$v(\omega) = \frac{l}{t_0 + d(\phi(\omega))/d\omega}$$

where

- $v(\omega)$ velocity of propagation;
- l effective length of line (2 × physical length);
- t_0 low-frequency time delay of line;
- $\phi(\omega)$ phase shift in radians.

While the measured and calculated attenuation agree well at low frequencies, there is significantly more measured attenuation at high frequencies. This increased attenuation is probably due to surface roughness of the copper line which causes an increasing effective resistance at higher frequencies because the current is confined to thinner surface depth due to skin effect. Because of the relatively small amount of phase shift observed for the 10 in of microstrip it is difficult to ascertain whether the observed shifts are due to real dispersive material effects or whether they are due to residual system effects (e.g., differences in the effectiveness of the shorts used in the 5-in and 10-in measurements). A second independent measurement (perhaps using somewhat longer lines) is needed to resolve the two effects.

B. RG/U 58 Coaxial Cable

Loss and dispersion results obtained for a 4-ft length of RG/U 58 cable are shown in Fig. 4(a) and (b). Also shown in Fig. 4(a) are the calculated copper loss and three published values for the total cable loss. In this case, corrections for the interface losses were necessary. These corrections amounted to less than 0.25 dB of the total observed attenuation at all frequencies. The attenuation up to 1.0 GHz is primarily conductor loss. Agreement with the published values is excellent. Fig. 4(b) indicates that dispersion above 6 GHz is significant.

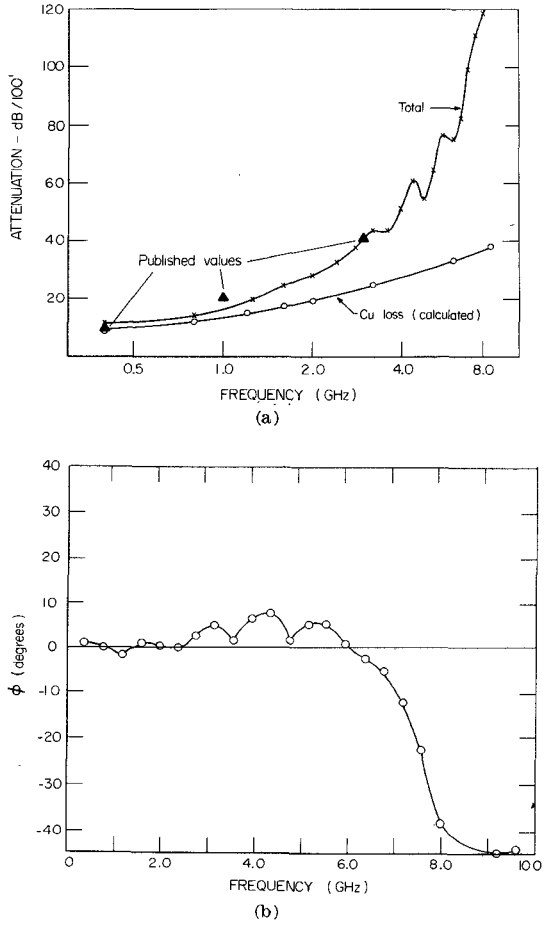

Fig. 4. Attenuation and normalized phase shift versus frequency for RG/U 58 coaxial cable. (a) Measured and calculated attenuation. (b) Normalized phase shift.

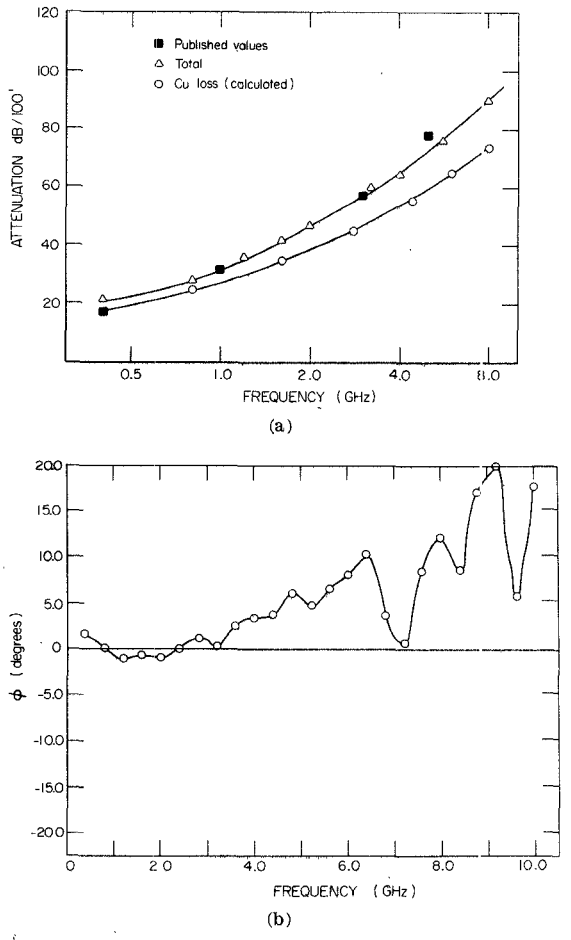

Fig. 5. Attenuation and normalized phase shift versus frequency for RG/U 188A miniature coaxial cable. (a) Measured and calculated attenuation. (b) Normalized phase shift.

C. RG/U 188A Coaxial Cable

Results obtained for a 3.8-ft section of RG/U 188A miniature PTFE coaxial cable are shown in Fig. 5(a) and (b). Agreement with published attenuation values is excellent. Losses in this cable are clearly dominated by conductor losses as indicated by the calculated copper loss curve. Fig. 5(b) shows the normalized phase shifts of the cable to 10 GHz. Dispersion, even at 10 GHz, is small.

IV. CONCLUSIONS

Results have been presented in the 0.4–10-GHz frequency range for transformed time-domain measurements of transmission line attenuation and dispersion which show good agreement with published values. Because of the time separation between multiple returns, errors due to interface discontinuities can be evaluated and removed from the final data. The measurements presented were limited to 10 GHz, essentially because of decreasing higher frequency signal-to-noise ratio of the smoothed impulse. However, with recent advances in pulse generators [6] it should be possible to extend the upper frequency limit to 18 GHz. The techniques can also be applied to other cable measurements such as crosstalk.

REFERENCES

[1] B. M. Oliver, "Time domain reflectometry," *Hewlett-Packard J.*, vol. 15, Feb. 1964.
[2] A. M. Nicolson, C. L. Bennett, Jr., D. Lamensdorf, and L. Susman,

"Applications of time-domain metrology to the automation of broadband microwave measurements," *IEEE Trans. Microwave Theory Tech. (Special Issue on Automated Microwave Measurements)*, vol. MTT-20, pp. 3–9, Jan. 1972.
[3] H. M. Cronson and G. F. Ross, "Current status of time-domain metrology in material and distributed network research," *IEEE Trans. Instrum. Meas. (1972 Conf. on Precision Electromagnetic Measurements)*, vol. IM-21, pp. 495–500, Nov. 1972.
[4] H. M. Cronson, P. G. Mitchell, and J. L. Allen, "Time domain metrology study," U. S. Army Missile Command, Redstone Arsenal, AL, Final Rep.–Phase I, SRRC-CR-72-9, Aug. 1972.
[5] R. A. Pucel, D. J. Massé, and C. P. Hartwig, "Losses in microstrip," *IEEE Trans. Microwave Theory Tech.*, vol. MTT-16, pp. 342–350, June 1968.
[6] H. M. Cronson, P. G. Mitchell, J. L. Allen, H. Strenglein, and R. L. Earle, "Time domain metrology study," U. S. Army Missile Command, Redstone Arsenal, AL, Final Rep.–Phase III, SCRC-CR-74-1, Jan. 1974.

Real-Time Fourier Analysis of Spread Spectrum Signals Using Surface-Wave-Implemented Chirp-Z Transformation

GRAHAM R. NUDD, SENIOR MEMBER, IEEE, AND OBERDAN W. OTTO, MEMBER, IEEE

***Abstract*—In many communication and radar applications it is desirable to determine the spectral content of signals in real time. A technique employing dispersive surface acoustic wave devices to implement the chirp-Z transform is described. The experimental results obtained for a number of commonly used signals, including the maximal-length pseudonoise sequences, are shown, and the agreement with theoretical prediction is discussed.**

INTRODUCTION

In many electronic systems a knowledge of the spectral content of received signals in real time provides an invaluable tool which allows the detection process to be rapidly optimized. Correlation receivers, matched filter detection schemes, and systems exhibiting high Doppler shifts are specific examples.

The advent of fast-Fourier-transform techniques has greatly speeded the spectral analysis in recent times, reducing the number of required operations for an N-point transform from N^2 to $N \log_2 N$. However, the cost and power requirements of high-speed digital circuitry has limited its applications in those instances where high speed and low cost are more important than high accuracy. The chirp-Z transformation provides a technique which can be inexpensively implemented using surface acoustic wave devices. In addition to the larger bandwidths, hence higher processing rates available in surface wave devices, the number of operations required for an N-point transform in a chirp-Z transversal filter implementation is N.

Implementation of the chirp-Z algorithm on surface wave devices has been demonstrated with Nyquist rate sampling on a periodically tapped delay line [1] and with continuous sampling in linear FM filters [2], [3]. The implementation utilized here is of the continuous sampling type.

CONCEPT OF TECHNIQUE

A number of authors have pointed out that the Fourier transformation can be expressed in the form of a convolution [4]–[6]. Mertz observed [4] that the operation of multiplication by a chirp prior to Fresnel transformation (convolution with a chirp), and postmultiplication by a chirp corresponds to Fourier transformation. A Fourier transform performed in this manner is referred to as a chirp-Z transform [5]–[6].

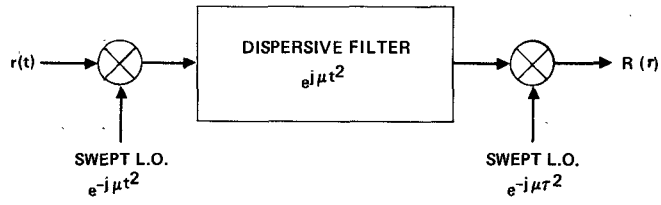

Fig. 1. Schematic of chirp-Z transform.

A linear FM filter of chirp rate μ provides the Fresnel transform $S(\tau)$ of the input $s(t)$

$$S(\tau) = \int dt\, s(t) \exp\left[j\mu(t-\tau)^2 \right]. \tag{1}$$

If the input to the filter $s(t)$ is the signal $r(t)$ multiplied by a chirp

$$s(t) = r(t) \exp\left[-j\mu t^2 \right] \tag{2}$$

and the filter output is also multiplied by a chirp

$$R(\tau) = S(\tau) \exp\left[-j\mu \tau^2 \right] \tag{3}$$

then the final output $R(\tau)$ is the Fourier transform of the input $r(t)$

$$R(\tau) = \int dt\, r(t) \exp\left[-j(2\mu\tau)t \right]. \tag{4}$$

The transformed function $R(\tau)$ appears in real time with the transform frequency proportional to time, the chirp rate μ being the proportionality constant. The chirp-Z implementation of the Fourier transform is illustrated diagramatically in Fig. 1.

EXPERIMENTAL IMPLEMENTATION

In the implementation discussed here, the final mixer stage was not included. This is because the output was displayed in video form and the phase of the carrier was not important. However, if further processing is required before detection, the final de-chirp stage may be required.

Dispersive surface acoustic wave devices were used both for generation of the swept local oscillator signal and for the convolution filter. The devices used had relatively modest time–bandwidth products of 40 with approximately 8-μs dispersion and 5-MHz bandwidth centered at 30 MHz.[1] The input to the first mixer was derived from either a function generator or a programmable data generator with bit rates up to 2 Mbit/s.

The output for a test signal of a single sinusoid of 1 MHz is shown in Fig. 2(a) together with the resulting transform. The transform can be seen to consist of 2 components at frequencies corresponding to ± 2 MHz.

The scanned bandwidth is limited by the filter bandwidth and the number of resolution cells within this is equal to the filter time–bandwidth product. Hence the maximum attainable frequency resolution (f_R) is given by

$$f_R = \frac{\mathrm{B}}{\mathrm{B} \times \tau} = \frac{1}{\tau} = 125\ \mathrm{kHz}.$$

In Fig. 2(b), the results for the same sinusoid with a dc bias are shown, and the corresponding zero frequency component can be seen in the transform. Distortion of the sinusoid is also evident, resulting in second-harmonic spectral components.

Manuscript received May 8, 1975; revised July 24, 1975.
The authors are with the Hughes Research Laboratories, Malibu, CA 90265.

[1] The dispersive delay lines used in this work were designed by the Ground Systems Group, Hughes Aircraft Company, Fullerton, CA.